MECHANIKA TEORETYCZNA
I STOSOWANA
Journal of Theoretical
and Applied Mechanics
2, 30, 1992

APPLICATION OF SUPERIMPOSED HOLOGRAPHIC INTERFEROMETERS IN EXPERIMENTAL MECHANICS

VITALII A. ZHILKIN

Chelyabinsk, Russia

In this review paper we discuss the methods of the investigation of various problems of mechanics by means of superimposed holographic interferometers. Investigations were carried out at the Novosibirsk Institute for Engineers of Railway Transport and the Chelyabinsk Institute for Mechanization and Electrification of Agriculture. Both the traditional and new method of analyzing of interferometric patterns reconstructed from a hologram recorded at a distance of a few centimeters from the surface of an object are described. Examples are given illustrating studies of fields of elastic and plastic strains, in strips with concentrators tested for axial stress under static and cyclic (few cycles only) loading, in shell–structures under axial load as well as under internal pressure.

1. Superimposed interferometers

The commonly used arrangements for recording holographic interferograms with a holographic plate and an object under study, both spread in space, have two serious inherent drawbacks which prevent holographic interferometry from industrial application.

1. Strict requirements for the vibration–safe insulation of experimental installations make it difficult to apply the standard testing equipment for loading samples, mashine parts and mechanisms.

2. The errors in determining displacements in the objects plane due to small aperture angle exceed considerably those observed in out–of–plane displacements.

Superimposed holographic interferometers are free from the above mentioned drawbacks since the holographic plate is attached to the surface of the object under study while holographic interferograms are recorded in opposed beams, according to the method suggested by Yu.N.Denisyuk (Fig.1) [1].

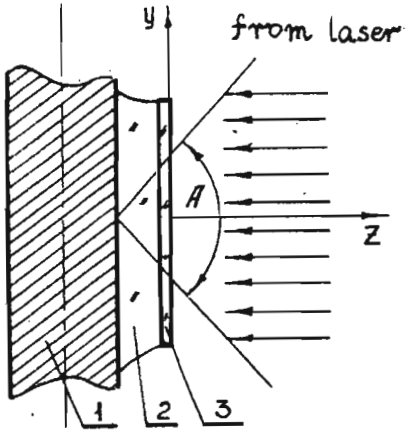

Fig. 1. Diagram of a superimposed holographic interferometer: A – aperture angle, 1 – the object under study, 2 – intermediate optical medium (rubber or air), 3 – photoplate (with the resolution range above 3500 lines/mm)

In this case it is possible to improve the accuracy of the determination of displacement vector components in the plane tangent to the surface of the studied object due to a larger aperture angle of a hologram and also due to special procedures, concerning the increasing of the diffraction angles of the surface under study.

In order to increase the aperture angle A and to improve the quality of interference pattern (IP), high frequency metallized gratings are placed on the surface of the object under study, before recording a hologram. This is done by the following procedure.

First, a holographic plate of high resolutiuon is placed into a stationary interference field of required frequency and the grating is recorded. After developing the photoplate a metal is dispersed on its emulsion layer (in most cases aluminium is used). By glueing the photoplate to the metal layer on the considered area of the sample surafce with the help of epoxy resin and tearing the glass plate afterwards one can get a mirror–like high frequency grating on the sample surface [2].

While studying the strain of massive objects mechanical or magnetic clamps are used to hold the holographic plate [3,4]. On this purpose for thin–walled structures, the intermediate optical media (IOM) are used. They do not change their optical and mechanical properties during the experiment and act as a layer since their shear rigidity is smaller than that of the holographic plate and the object under study. A plate cemented to the surface of the object by means of IOM should not considerably distort the field of strains under study. IOM has a smaller weight than that of the clamping device. Consequently it allows for certain tolerable

displacement of the object and does not cause the errors in determining the values of membrane strains. Besides it minimizes the requirements to the vibration–safe insulation of the object under study, and finally, the influence of displacements W on an interference pattern, normal to the surface of the holographic plate, is reduced due to the presence of adhesive forces between the holographic plate and the surface of the object. The use of IOM allows carrying out the investigation of strains of various structures and objects by means of holographic methods, recording information in industrial environment, using standard testing equipment. [5 ÷ 18].

The holographic plate should allow recording of holograms in opposed beams. The use of holographic films and IOM facilitates the study of the state of the developable surfaces. There are no special requirements for the quality of the surface of the object under study in using superimposed interferometers. To improve the accuracy of determining in–plane displacements of the object it is desired to approximate the surface dissipation indicatrice by a sphere because the superimposed interferometers make it possible to observe interference patterns in the whole range of $\pm\pi/2$ of a hemisphere.

It is known that when recording double–exposure holograms at the surface of a metallized grating, we can observe (both on transmission and reflection) four types of interference patterns: in illuminating the hologram by means of a plane wave and in scanning it with an unspread laser–beam. The analysis of these interference patterns in this case results in strain fields, practically, with the same accuracy. However when the surface of a machine part is not flat and has indents, holes etc., it is not possible to use traditional methods of analysis of fringe patterns, observed in scanning hologram with an unspread laser–beam since they might result in considerable errors in determining the strains. In this paper we describe both the traditional and new methods of analysis of interference patterns, restored by a hologram, recorded at a distance of a few centimeters from the object surface. There are examples of elastic and plastic strain fields for plates with notches, tested for axi–symmetrical strain both by static and low cycle loads in the plates, tested for bending, in shell structures by axial compression and loaded with internal pressure.

2. Types of interferometers

For the sake of clarity let us assume, that the axes x and y of the Cartesian system of coordinates are aligned with the surface of the holographic plate and axis z is directed along the external normal to the surface of an object. The projections of the displacement vector $\Delta\mathbf{r}$ on the coordinate axes x, y and z are denoted by U, V and W respectively, and the directional cosines of the observation angle (o)

and illumination (l) are defined as

$$l_i = \cos\alpha_i \qquad m_i = \cos\beta_i \qquad n_i = \cos\gamma_i \qquad (i = o, l)$$

Changing the shear rigidity both of the IOM and the substrate of the photographic emulsion, as well as methods of the preparation of the surface of the studied object, we can get four different types of interferometers A, B, C and D, the schematic representation of which is shown in Fig.2 [18].

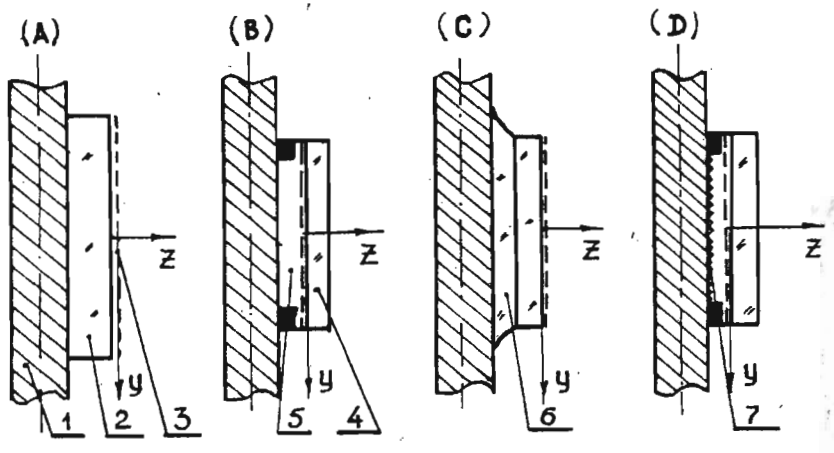

Fig. 2. Types of interferometers: 1 – the object under study, 2 – non–birefringent plexi–glass, 3 – piezoregistering medium, 4 – glass base, 5 – air gap, 6 – intermediate optical medium, 7 – metallized reflecting grating

It is well known, that a general equation of holographic interferometry method, is as follows

$$\Delta\boldsymbol{r} \cdot \boldsymbol{k} = N\lambda \tag{2.1}$$

where $\Delta\boldsymbol{r} = U\boldsymbol{i} + V\boldsymbol{j} + W\boldsymbol{k}$; $\boldsymbol{k} = \boldsymbol{\rho}_l - \boldsymbol{\rho}_o$; $\boldsymbol{\rho}_\tau = l_\tau\boldsymbol{i} + m_\tau\boldsymbol{j} + n_\tau\boldsymbol{k}$ $(\tau = l, o)$ are unit vectors of observation and light angles (l) and (o); N is the order of interference fringes; λ – is the wave length of the light.

In interferometers B, C and D the photographic emulsion is placed on the non–deformable substrate and in interferometers type A – on the deformable one.

When the plane stress state is realized, for which displacements of points U and V of the surface object and the holographic plate are equal, an interferometer of type A can only register the changes of thickness t of the coating. The interference fringes pattern, obtained by the double–exposure hologram will carry the information, concerning the sum of principal strains. From Eq (2.1) it results

$$W = \frac{N\lambda}{2n}$$

and since

$$\varepsilon_z = \frac{W}{t} = -\frac{\mu(\varepsilon_x + \varepsilon_y)}{1-\mu}$$

we obtain

$$\varepsilon_x + \varepsilon_y = -\frac{(1-\mu)N\lambda}{2nt\mu} \tag{2.2}$$

where μ – Poisson ratio; n – is the refractive index of the coating material.

Fig.3 gives us the isopachic and the diagram of the sum of the strains $(\varepsilon_x + \varepsilon_y)$ in the cross–sections (1 and 2) of the sample. On a flat sample, 1.75 mm thick, made of alluminum alloy D16T (Young modulus $E = 7 \cdot 10^4$ MPa) the sheet of the plexiglass 1.24 mm thick ($E = 3 \cdot 10^3$ MPa) was glued, on which a photographic emulsion of high resolution was dispersed. The fringe order at points at considerable distance from the concentrator was defined by the mean value of strains in the same sections of the sample. The sun of the strains $(\varepsilon_x + \varepsilon_y)$ in the cross–sections 1 and 2 of the sample was calculated on the basis of Eq (2.2). In the cross–section 1 the experimental results were compared with those of numeric calculations, carried out on the basis of relations, given in [19]. The comparison of results was satisfactory.

Further we shall discuss only the interferometers of types B, C and D since they are the simplest and can be easily made in any laboratory. The resolution equations of these interferometers will be given below.

In most of our works as a support of holographic plate silicon rubber type CKTH–A was used, hardened at normal room temperature by means of the catalytic agent K–18. Optimization of the rubber composition and the modes of its production were realized. Certain stable parameters of the medium (transparency, refraction factor, elasticity modulus) can be achieved by correlation of weight of the rubber and the catalytic agent (ratio 100:1 [20]). By studying the strain, approximating the static state, or characterized by the frequencies less than 0.1 Hz, we can assume, that the holographic plate is immovable with respect to the sample and, as a result, the holographic interferogram registers only the real displacement field of the sample. For frequencies exceeding 0.1 Hz, the motion of the photoplate with respect to the sample cannot be neglected. However, in using CW lasers and in solving the static problems the noise interference pattern during the exposure of the holographic plate is averaged and it will not cause errors in the displacement fields. In a case when a pulsed laser is used, the registered interference pattern will correspond to the sum of the displacement fields, that under study and induced by the vibrations of the testing equipment [5].

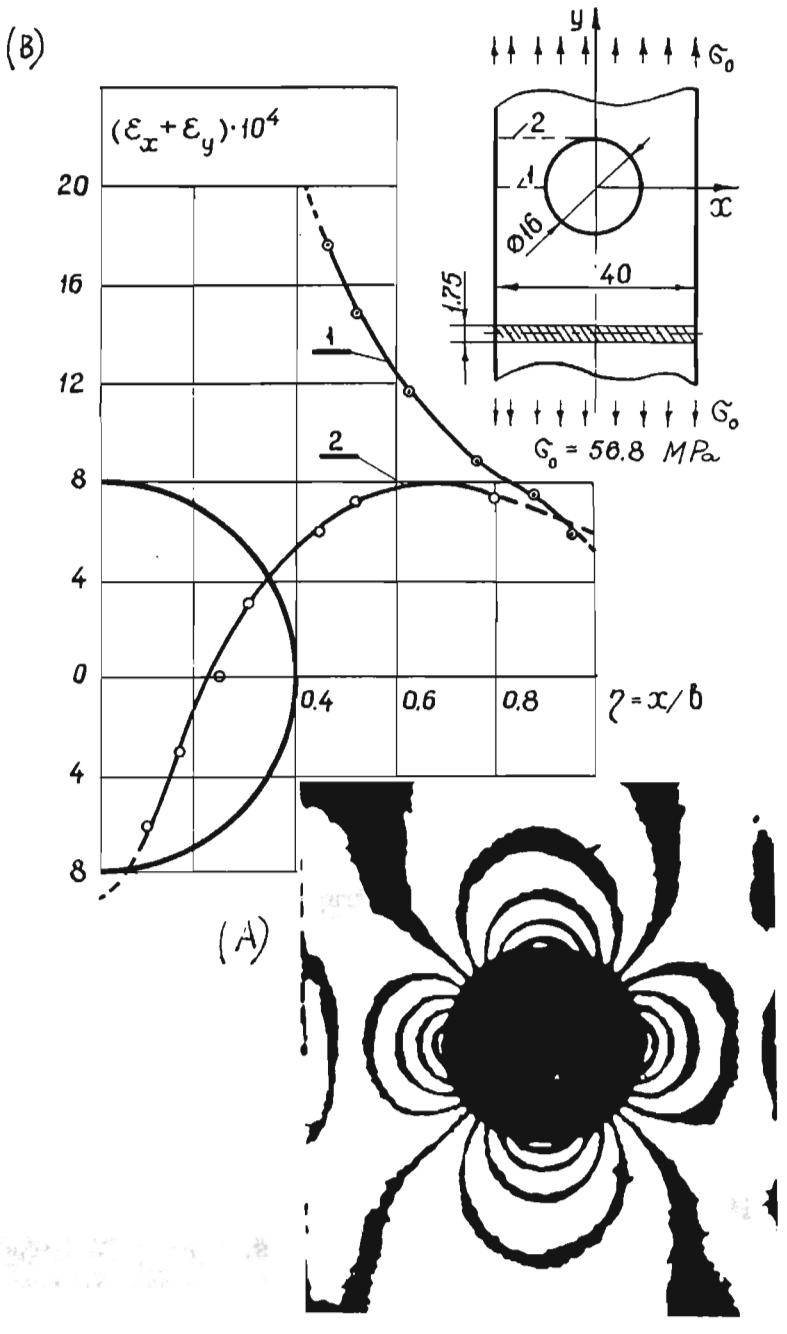

Fig. 3. Pattern of isopachics (A) and diagrams of the sums of strains $(\varepsilon_x + \varepsilon_y)$ in cross-section 1 and 2 of the sample (B)

3. Analysis of the interference patterns

If a high resolution photographic emulsion is placed in the vicinity of the surface under study, having high reflectivity and if both are illuminated by a coherent plane wave, then as a result of the cross–interference of the reference beam and the object beam the photographic emulsion will record gratings of the RO–type, responsible for the interference patterns, observed on the reflection and 00–gratings, responsible for optical patterns, observed at transmission (Fig.4).

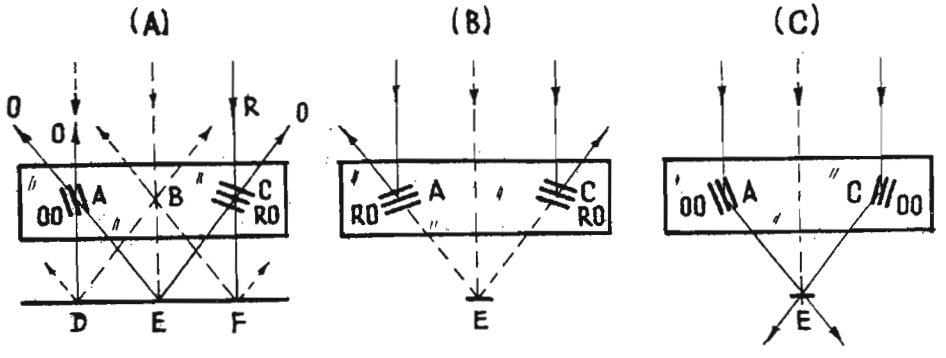

Fig. 4. Diagram of recording holograms in opposing beams (A) and schemes of observation of optical patterns on reflection (B) and on transmission (C)

For interference patterns, observed on the reflection in the vicinity of point E (Fig.4B), the equation has the following form

$$U_E l_o + V_E m_o + W_E\left(n + \sqrt{n^2 - \sin^2\gamma_o}\right) = N_r\lambda \tag{3.1}$$

and for the optical patterns, observed at the transmission (Fig.4C) equation is [21]

$$U_E l_o + V_E m_o - W_E\left(n - \sqrt{n^2 - \sin^2\gamma_o}\right) - 2R = N_t\lambda \tag{3.2}$$

where $R = f(H, \gamma_o, W)$ is the residual member of Taylor series, n – is the refractive index of the intermediate optical medium (for air $n = 1$); N_r, N_t – are fringe orders on the reflection and at the transmission respectively; H is the distance between the sample surface and the photographic emulsion.

By simultaneous illumination on the whole plane of the double–exposure hologram by a plane wave we can observe at an arbitrary point of the object as seen from different direction, whereas the components U_E, V_E, W_E in Eqs (3.1) and (3.2) remain the same, while only the directional cosines and fringe orders change. It permits to determine the sought–for displacements U_E, V_E, W_E using 4 pairwise

observation angles symmetrical with respect to the axis z. The strain components are determined by numeric differentiation in accordance with Cochy correlations.

At scanning such double-exposure hologram with an unexpanded laser-beam you can see on the screen, positioned near the hologram, an image of the area of the studied surface in the diffraction halo (Fig.5), covered by a certain system of fringes, while the screen, placed at a considerable distance from the hologram, shows the system of fringes, inherent in the traditional method of speckle-photography, due to the decrease of the aperture. Thus, we can observe different parts of the object from a single point B, and that is why in Eqs (3.1) and (3.2) the displacement components U, V and W are different for different directions of observation. Therefore we cannot make use of Eqs (3.1) and (3.2) directly.

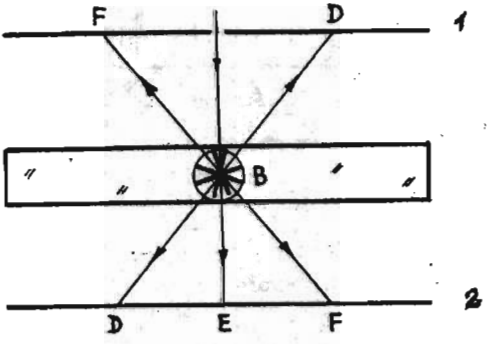

Fig. 5. Diagram of scanning holograms by an unexpanded laser beam: 1 – screen on reflection, 2 – screen on transmission

Expressing random points displacement by the displacement of point E with the help of Tylor series and transforming correlations (3.1) and (3.2), we shall get the following resolution equation [22]: for the fringe patterns, observed at the reflection

$$U_E l_o + V_E m_o + W_E(1 + n_o) + A = N_r \lambda \tag{3.3}$$

for interference patterns, observed at transmission

$$U_E l_o + V_E m_o + W_E(1 + n_o) - 2W_E + A = N_t \lambda \tag{3.4}$$

$$A = \left[(\mathrm{grad} U_E) l_l + (\mathrm{grad} V_E) m_l + (\mathrm{grad} W_E)(1 + n_l)\right] \cdot d\boldsymbol{\rho}_{xy}$$

$$\mathrm{grad} R = \frac{dR}{dx}\boldsymbol{i} + \frac{dR}{dy}\boldsymbol{j} \qquad (R = U_E, V_E, W_E)$$

$d\boldsymbol{\rho}_{xy} = \boldsymbol{i}dx + \boldsymbol{j}dy$ – radius-vector, defining the position of a point on the sample surface with respect to the scanning point.

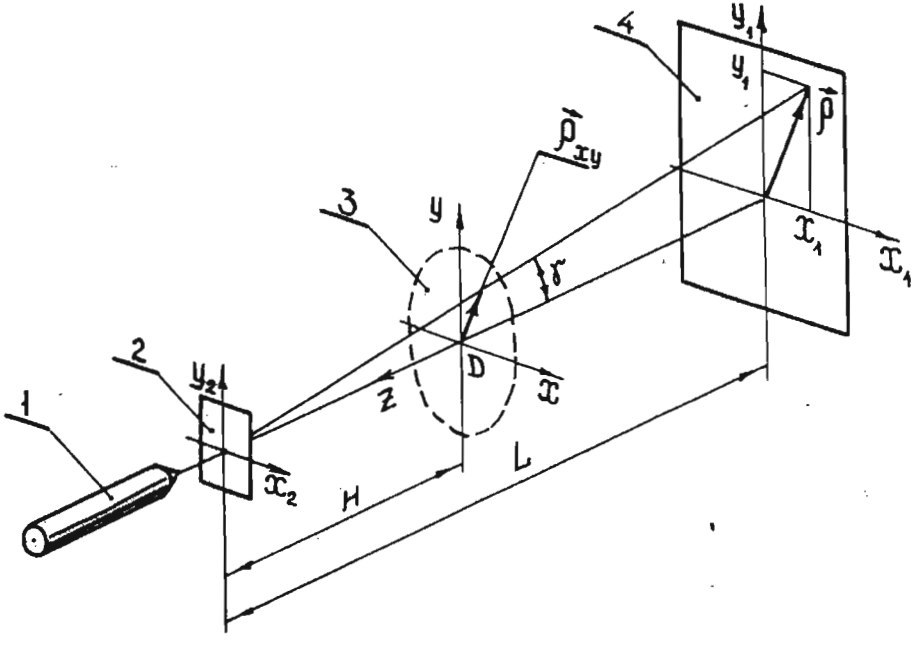

Fig. 6. Diagram of scanning of the double–exposure holograms by Denisyuk

As an example, new resolution equations and correlations can be derived from Eqs (3.3) and (3.4) that can be used within the traditional method of speckle–photography. At the same time we must consider the fact, that during recording of a hologram the holographic plate was placed at distance H from the sample surface, and the screen was at the distance L ($L > \rho$, $L > x$, $L > y$) (Fig.6) from the hologram, that is why the coordinates x and y of the sample surface points are connected with the coordinates of the corresponding points on the screen surface by the correlations

$$x_1 = Mx \qquad y_1 = My \tag{3.5}$$

where $M = L/H$ is the pattern scale of the sample surface in the plane $x_1 y_1$ and the directional cosines can be calculated by the following formulae

$$\cos\gamma = \frac{L}{\sqrt{L^2+\rho^2}} = \frac{1}{\sqrt{1+(\rho/L)^2}} = 1 - \frac{(\rho/L)^2}{2}$$
$$\cos\alpha = \frac{x_1}{\sqrt{L^2+\rho^2}} = \frac{x_1}{L}\cos\gamma \tag{3.6}$$

$$\cos\beta = \frac{y_1}{\sqrt{L^2+\rho^2}} = \frac{y_1}{L}\cos\gamma$$

In case when it is possible to consider constant values of U, V and W within the limits of the diffraction halo, Eqs (3.3) and (3.4) become somewhat simpler. When γ is small and when correlations (3.6) are taken into consideration, Eq (3.4) will assume the form

$$Ux_1 + Vy_1 = N\lambda L \tag{3.7}$$

It means in plane x_1y_1 we can observe a system of equidistant straight lines. Let us assume, that a certain point in coordinates (x_1, y_1) is positioned on the first fringe (in Eq (3.7) $N = I$), then

$$Ux_1 + Vy_1 = \Delta\boldsymbol{r}\cdot\boldsymbol{\rho} = \Delta r\, a$$

where a is the interference fringes pitch and we shall have the commonly known correlation.

When $U = 0$, $V = 0$ and $W \neq 0$ functions (3.3) and (3.4) take the form

$$W(1+\cos\gamma) = N\lambda \tag{3.8}$$

$$-W(1-\cos\gamma) = N\lambda \tag{3.9}$$

If we consider that the interference fringes order N is determined with an accuracy to a digit, it might be possible to find out the radii ρ of the concentric interference fringes. Thus we see on the diagram (Fig.7A)

– for reflection

$$\rho = L\,\mathrm{tg}\,\arccos\left(-1 + N\frac{\lambda}{W}\right) \tag{3.10}$$

– for transmission

$$\rho = L\,\mathrm{tg}\,\arccos\left(1 - N\frac{\lambda}{W}\right) \tag{3.11}$$

where $N > 0$.

If the angle γ is small, Eqs (3.8) and (3.9) can be simplified

$$W\left(2 - \frac{\rho^2}{2L^2}\right) = N\lambda \tag{3.12}$$

$$W\frac{\rho^2}{2L^2} = N\lambda \tag{3.13}$$

then formulae (3.10) and (3.11) assume the form

$$\rho = L\sqrt{2\left(2 - N\frac{\lambda}{W}\right)} \tag{3.14}$$

In this case

$$\varepsilon_x = \frac{\partial U}{\partial \hat{x}} = \frac{\partial U}{\partial x} \qquad U = \varepsilon_x \hat{x}$$

$$V = -\mu\varepsilon_x \hat{y} \qquad W = 0 \qquad \mathrm{grad}W = 0$$

and Eqs (3.3) and (3.4) are converted to the form

$$\left(U + \frac{\partial U}{\partial \hat{x}} d\hat{x}\right)\cos\alpha + \left(V + \frac{\partial V}{\partial \hat{y}} d\hat{y}\right)\cos\beta = N\lambda$$

Here ε_x is the strain of the sample material in the direction of axis x; μ is the Poisson ratio; $\hat{x}, \hat{y}$ are the coordinates of the scanning point ($\hat{x} = x_B$, $\hat{y} = y_B$) of the hologram. In the local systems of coordinates xyz and $x_1y_1z_1$ connected with point B

$$d\hat{x} = x = H\frac{x_1}{L} \qquad d\hat{y} = y = H\frac{y_1}{L}$$

Thus, in the diffraction halo on the screen we shall see a system of interference fringes, described by the equation

$$\left(U + \varepsilon_x H\frac{x_1}{L}\right)\frac{x_1}{L} + \left(V - \mu\varepsilon_x H\frac{y_1}{L}\right)\frac{y_1}{L} = N\lambda \tag{3.16}$$

If the gap between the photoplate and the sample is small ($H \sim 0$) then there will be a system of equidistant straight lines on the screen $Ux + Vy = N\lambda L$, the equation of which is similar to (3.7) and, consequently, it is possible to use the traditional ratio to determine displacement U and V.

By $H \neq 0$ on the system of equidistant straight lines, described by Eq (3.7), in which we should put down $N = N_1$, the hyperbolic fringes will be superimposed in accordance with Eq (3.16)

$$\frac{\varepsilon_x H}{L^2}(x_1^2 - \mu y_1^2) = N_2\lambda \tag{3.17}$$

where $N_2 = N - N_1$. Hyperbolic fringes in their clear form will be observed at the point, coinciding with the origin of the coordinate system $\hat{x}\hat{y}\hat{z}$.

If we consider the strain of strip of average thickness, the displacements of points on their surface are described by the correlations [26]

$$U = -\frac{h}{2}\frac{\partial W}{\partial x} \qquad V = -\frac{h}{2}\frac{\partial W}{\partial y} \tag{3.18}$$

where h is the thickness of a strip.

We shall substitute (3.18) into Eqs (3.3) and (3.4). Here we assume that angle γ is small, when $h \ll L$. In this case the interference patterns are described by the equations

– on reflection

$$W\left(2-\frac{\rho^2}{2L^2}\right)+\frac{2H-h/2}{L}\left(x_1\frac{\partial W}{\partial x}+y_1\frac{\partial W}{\partial y}\right)=N\lambda \tag{3.19}$$

– on transmission

$$\frac{W\rho^2}{2L^2}+\frac{2H-h/2}{L}\left(x_1\frac{\partial W}{\partial x}+y_1\frac{\partial W}{\partial y}\right)=N\lambda \tag{3.20}$$

When H ($H \to 0$) is small, Eqs (3.19) and (3.20) coincide with correlations (3.12) and (3.13). If H is comparable with L then the component $(-W\rho^2/(2L^2))$ in Eqs (3.19) and (3.20), while compared with the remaining can be neglected. In the latter case, interference fringes patterns, that we see on the screen, represent a system of equidistant straight lines.

Now we can carry out an experimental test of the validity of the proposed equations.

3.1. The displacement along the axis z of the object under study, taken as a rigid body

A metal plate was fastened to the table of the mircoscope at 3.5 mm from the surface, then, during the time between two exposures, the plate was displaced along the optical axis (along the axis z) at a step of $W = 77$ μm.

Interference fringes reconstructed from the hologram by reflection and transmission have the form of the system of concentric circles (Fig.7A). The plane of the screens were positioned at distance $L = 180$ mm and $L = 174$ mm from the hologram respectively.

Fig.8 shows the comparison of the results of the calculated radii of the dark interference fringes according to formulae (3.10), (3.14), (3.11), (3.15), as well as the experimental results. The continuous curve corresponds to Eq (3.10), the dotted curve – to Eq (3.11), the triangle corresponds to Eq (3.14), the dark circle – to formula (3.15), the light circle – to the experimental results, obtained from the interference fringes patterns as seen at the transmission and the crosses correspond to the experimental results, obtained from the interference fringes pattern as seen for the reflection. Up to $N = 8$ (235) the results of calculations according to formulae (3.10) and (3.14), (3.11) and (3.15) are practically the same. Therefore, when $\gamma < 20°$ in the process of analysis of the interference pattern, we can use (3.14) and (3.11). The coincidence of the radii of the dark interference fringes within the limits of the observed interference pattern, calculated on the basis of Eqs (3.10) and (3.11) and experimentally measured, is satisfactory.

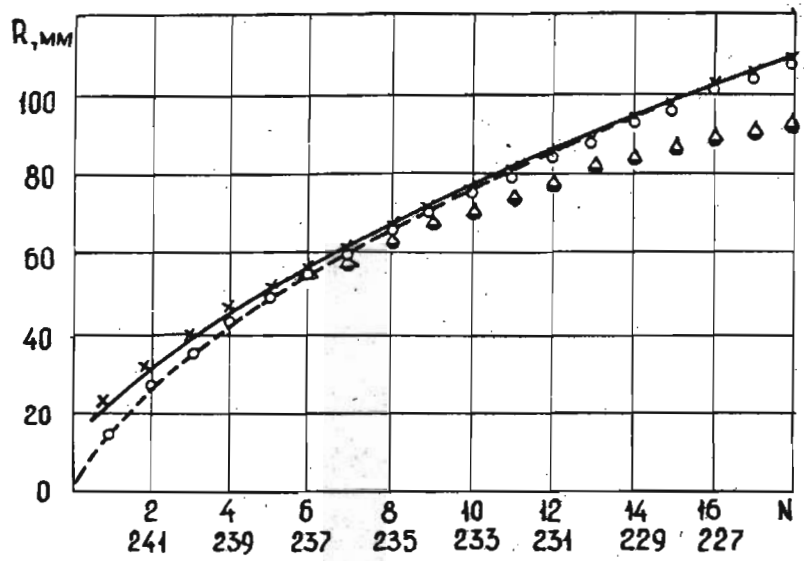

Fig. 8. Diagram showing the change of fringe orders along the coordinate x

3.2. Axial tension of a flat plate

The study was carried out to check the correlation (3.16). Let us determine the strains ε_x and ε_y using the data obtained by illuminating a hologram at one point and then to calculate the elastic properties of the material.

Double–exposure hologram was recorded at the distance $H = 9.3$ mm from the plate surface reflecting the light within diffusion. The plate was made of aluminium alloy D16T. The dimensions of the cross–section of the plate are 40mm × 1.8mm. During the time between two exposures the plate was loaded with the force of 5 kN.

Fig.7B shows the interference pattern observed at reflection, representing an interference of the families of hyperbolic and straight lines (see Eqs (3.17) and (3.7)). It is rather difficult to determine the point at which $U = 0$ and $V = 0$, hence 4 unknown values U, V, ε_x and ε_y enter Eq (3.16). To determine them a system of 4 equations was solved, recorded for two points, lying on two adjacent interference fringes in either of the two orthogonal sections

1) $y_1 = 0$

$$\left(U + \varepsilon_x H \frac{x_1}{L}\right)\frac{x_1}{L} = N_1\lambda$$
$$\left(U + \varepsilon_x H \frac{x_2}{L}\right)\frac{x_2}{L} = N_2\lambda$$

2) $x_1 = 0$

$$\left(V + \varepsilon_y H \frac{y_1}{L}\right)\frac{y_1}{L} = N_3\lambda$$
$$\left(V + \varepsilon_y H \frac{y_2}{L}\right)\frac{y_2}{L} = N_4\lambda$$

Here x_1, x_2, y_1, y_2 are coordinates of the centres of the interference fringes with numbers N_1, N_2, N_3, N_4, respectively.

In our case $L = 342$ mm, $N_1 = 1$, $x_1 = 38$ mm, $N_2 = 2$, $x_2 = 67$ mm, $N_3 = 1$, $y_1 = 83$ mm, $N_4 = 2$, $y_2 = 142$ mm. As a results of calculation it were determined $\varepsilon_x = 9.6 \cdot 10^{-4}$, $\varepsilon_y = 2.8 \cdot 10^{-4}$, which differ from the given strain $\varepsilon_x = 9.9 \cdot 10^{-4}$ by 3%.

3.3. The investigation of the strain of the isotropic, rigidly clamped round plate, loaded by a continuous distributed load

The deflection W and rotation angles of such a plate are described by equations [26]

$$W = \frac{qR^4(1-\xi^2-\eta^2)^2}{64D}$$

$$\frac{\partial W}{\partial x} = -\frac{q\xi R^3(1-\xi^2-\eta^2)}{16D} \tag{3.21}$$

$$\frac{\partial W}{\partial y} = -\frac{q\eta R^3(1-\xi^2-\eta^2)}{16D} \tag{3.22}$$

where q is the intensity of the continuous load; R is the radius of the plate, $\xi = x/R$, $\eta = y/R$, $D = Eh^3/(12(1-\mu^2))$ is the bending rigidity. The origin of the coordinate system $0xy$ is placed at the centre of the plate.

The plate, representing the flat head of pressure vessel, loaded by internal pressure, was made of aluminium alloy D16T. The plate thickness was not constant, it ranged between 0.87 to 0.91 mm. In further calculations the boundary values 0.87 and 0.91 were used in calculation of the deflections of the plate.

The inner volume of the pressure vessel was filled with water and was connected to an external measuring tube. The loading of the plate was carried out by changing the column of water in the measuring tube between the expositions. The double-exposure hologram was recorded at the distance of $H = 9$ mm on the plate surface under $q = 3.3$ kPa. The fringe patterns, as seen at the transmission, were registered on the screen, positioned at $L = 545$ mm.

Fig.9A shows the diagrams of the rotation angles $(\partial W/\partial x)$ and $(\partial W/\partial y)$ at two cross-sections of the plate I and II (Fig.9B), calculated according to (3.21) and (3.22) as well as the data, obtained as a result of analysis of the optical patterns.

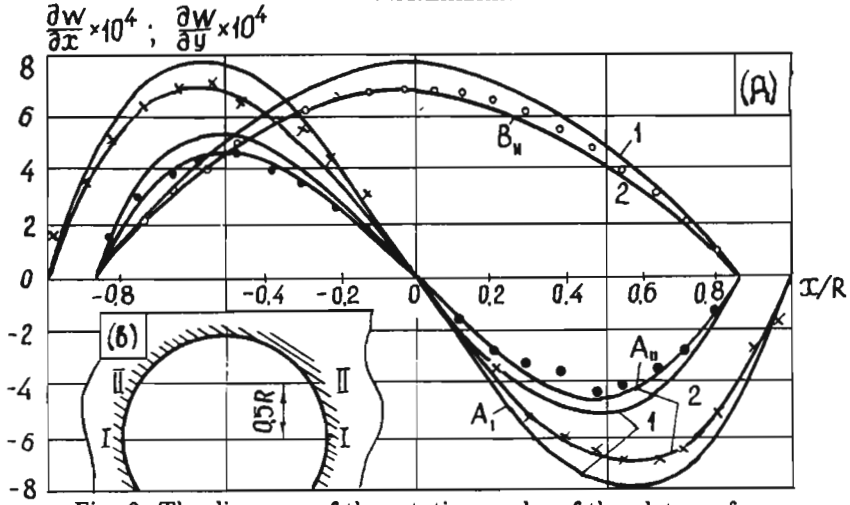

Fig. 9. The diagrams of the rotation angles of the plate surface

The diagrams denoted by 1, correspond to the plate thickness of 0.87 mm, while those denoted by 2 to the thickness 0.91 mm; the symbols: crosses, light and dark circles relate to experimental data the curves B_{II} correspond to the function dW/dy at the plate cross-section II–II, but curves A_I and A_{II} correspond to the function dW/dx at cross-sections I–I and II–II, respectively.

In calculation the rotation angles of the external plate surface on the basis of the experimental data Eq (3.20) was used, in which the influence of the first component of the form of the interference pattern was neglected. The rotation angles were calculated on the basis of the formulae

$$\frac{\partial W}{\partial x} = \frac{N_x \lambda L}{(2H - h/2)\Delta x_1}$$
$$\frac{\partial W}{\partial y} = \frac{N_y \lambda L}{(2H - h/2)\Delta y_1}$$

where Δx_1 and Δy_1 are the distances between N_x and N_y fringes along the axis x_1 and y_1, respectively.

The difference between the experimental data and the theoretical does not exceed 10 per cent.

Thus, in analysis of the patterns, observed when scanning the hologram by Denisyuk, Eqs (3.3) or (3.4) should be used. The correctness of the approximate equations has to be verified in each case, since it is necessary to take into account both the conditions of hologram recording, especially the distance between the object and the holographic plate and the strain character of the sample.

4. Automatization of experimental studies

The holographic interferometry is a method converting the change of optical path due to displacement or deformations into an optical signal. The range of displacements measured by this method

$$\frac{1}{S_D}\min\psi_i \le D \le \frac{1}{S_D}\max\psi_i \qquad (D = U, V) \tag{4.1}$$

is inversely proportional to its sensitivity S_U and S_V in observing the interference patterns in planes xz and yz, respectively

$$S_U = \frac{1}{\lambda}\sin\gamma_x \qquad S_V = \frac{1}{\lambda}\sin\gamma_y$$

where $\max\psi_i$ and $\min\psi_i$ are the maximal and minimal frequencies of the interference pattern defined by the level of averaging the strains on the basis of interference fringes and specifications of the equipment employed (most often, when we use traditional methods of optical patterns evaluation $\min\psi_i = 0.05$ lines/mm, $\max\psi_i = 1$ lines/mm). The numerator in experession (4.1) does not depend on the applied optical method.

For $\gamma_x = 30^\circ$ and $S_U = 790$ lines/mm, $D = (6 \div 200)\cdot 10^{-5}$, that is by means of the holographic interferometry it is possible to study only the elasticity problems, or to use it when studying the plastic strain of a material, together with other optical methods of lower sensivity. The use of MHI independently leads to the necessity to use the stage–by–stage methods for both loading a sample and recording interference patterns. If, for instance, it is necessary to study the strain of a bar made of aluminium alloy D16T and tested for axial tension, then it will be necessary to register four consecutive interferograms to reach the strains $\varepsilon_T = 4\cdot 10^{-3}$, corresponding to the plasticity level of the sample, since in this case each of the interferograms will exceed the strain limit $(0 \div 1.26)\cdot 10^{-3}$. To study the kinetics of the strain and failure of the sample it might be necessary to record about 200 interferograms. It is clear, that solving of such problems is closely connected with working out the ways of automatic analysis of the experimental information and creating algoritms of its processing by means of a computer.

The problem of analysing the information can be divided into three stages: loading information into computer memory and making a preliminary processing, determination of isolines of whole and fractional orders of fringes, fringe correction and numeration, analysis of fringe patterns.

In our investigation we used mini–computers, widely used in the 80's in the USSR – SM–4 and DVK–2M. The computers were equipped with the operational memory of 128K, two floppy–disk drives, a mosaic–type printer and a plotter [27].

The problem of processing and analysing optical patterns was organized as a dialogue process. Full automatization of the process was not possible.

The capabilities of the program can be illustrated by an example of the experimental information processing obtained while solving Kirsch's problem with the help of holographic interferometry method [27].

The sample made of aluminium alloy D16D had the following dimensions: length – 400 mm, width – 40.2 mm, thickness – 1.06 mm and it was loaded by axial force on a testing machine DM–30 M. A photoplate PE2 was fastened to surface of a sample with the help of intermediate optical medium SKTN–A. The interferogram was registered by a double–exposure method on reflection. Interference fringe pattern corresponding to the load increment of 2.8 kN is shown in Fig.10A. To load it into the computer we used a dot TV dissector with the diameter of the photocathode 100 mm and a aperture of 100 μm. The picture projected by the optics on the photocathode was quantized into 128 grey levels and was recorded into one of the zones of Operational Memory Device KAMAK in the form of a matrix having the dimensions 256 by 256 points. As the loaded fragment of the optical pattern was 40 by 40 mm, the picture fragment had linear dimensions of 156 μm. The recorded image was displayed on a black–and–white semi–toned monitor. Fig.10B shows a fringe pattern, corresponding to Fig.10A, displayed on the screen after preliminary processing of the pattern. Fig.10C shows a sceletonized pattern.

(A) (B) (C)

Fig. 10. Interference fringe patterns: (A) – stored in the computer memory, (B) – seen on the display, (C) – centres of interference fringes

The best results of processing a fringe pattern are obtained by using the boundary integral equations method [28]. In this case the information concerning the inteference fringes is given only on the contour surrounding the hole area, and then a problem of elasticity theory is solved in a traditional way. The use of boundary integral equations makes it possible to exclude the process of calculation of deriavatives on the basis of approximate values. The distribution of fixed strains

ε_x and ε_y in the critical cross–section of the strip with a round central hole is given in Fig.11.

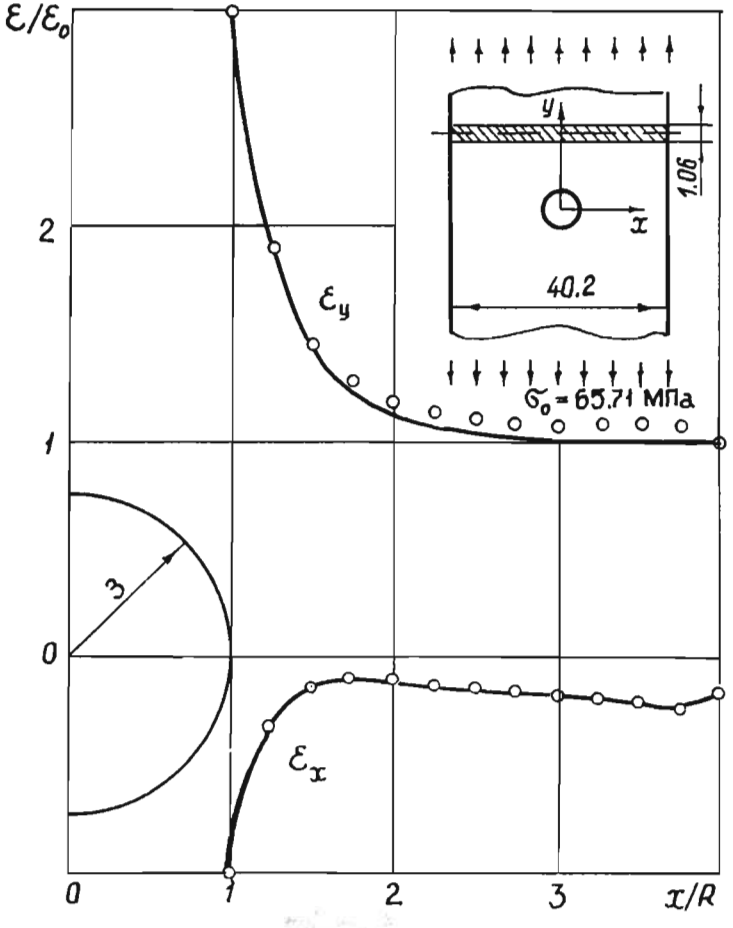

Fig. 11. Diagrams of strains at critical cross-sections of a strip: — - theoretical solution using the boundary integral equations method, o - experimental results

When solving spatial elastic and plane non–linear problems of mechanics it is advisable to use the holographic interferometry method in combination with the boundary integral equations. Such an approach was used in our study of the strain of the support unit of a non–metallic structure [11].

5. Examples of experiments

5.1. Selection of sensitivity of the experimental method [31]

Depending on the characteristic of the optical methods, e.g. the methods of moire, the holographic interference method and speckle–photography (as a variant of the fringe filtering method), we determine only the average strain on the basis of the distance of the interference fringe. In some cases the strains determined by means of this method can differ from the real ones considerably.

The loss of information about the true field of strains and the errors of its approximation will be reduced to a minimum, if the sensitivity of an optical converter is choosen according to the conditions that the linear displacement field approximation will lead to errors in determining the strains ε not exceeding 5%.

Errors in determining strains will not exceed 5% if the sensitivity of a converter satisfies the inequality

$$\psi > [\psi] = \sqrt{\frac{|\varepsilon''|}{1.2|\varepsilon|^3}} \tag{5.1}$$

where at all studied points of the sample surface the distance between interference fringes will be less, than the maximum acceptable one

$$f \leq [f] = \sqrt{\frac{1.2|\varepsilon|^3}{|\varepsilon''|}}$$

From Eq (5.1) it follows that studying of homogeneous and linear stressed states on the basis of interference patterns it is possible to restore exactly the strain field under study, and what is the most important, the ultimate sensitivity of a method is a function of the coordinates of the points of the surface of the sample. Therefore, by developing various optical methods one should not improve their sensitivity, but to work out methods of compensation of optical path difference, permitting to change the frequency of quantization and thus to measure the strains with desired accuracy.

When planning the experiment the researcher often does not know either ε or ε''. These values can be approximately defined after carrying out a "test". When you study the strain fields in locally strained zones using various concentrators as the first approximation, you can use either Kirsch's solution [26] or the solution determining the field of elastic stresses and displacement at the minor edge area of a random fracture [32]. In the case of Kirsch's solution, assuming $\mu = 0.3$ we shall get

$$f < 0.4R \tag{5.2}$$

$$\psi > \frac{0.8}{R\varepsilon_0} \tag{5.3}$$

where R is the radius of the hole, ε_0 – strain at a distance from the concentrator.

From Eq (5.3) it follows, that the less is the radius of the hole the higher must be the sensitivity of the method.

For holographic interference method the sine of the observation angle should satisfy the following inequality

$$\sin\gamma > \frac{0.8\lambda}{R\varepsilon_0} \tag{5.4}$$

For $\varepsilon_0 = 1 \cdot 10^{-3}$, $R = 1$ mm the observation angle should exceed 30^o, the similar result will be also for $\varepsilon_0 = 1 \cdot 10^{-4}$, $R = 10$ mm. For $\varepsilon_o = 1 \cdot 10^{-3}$, $R = 1$ mm at all possible observation angles there will be an irreversible loss of information.

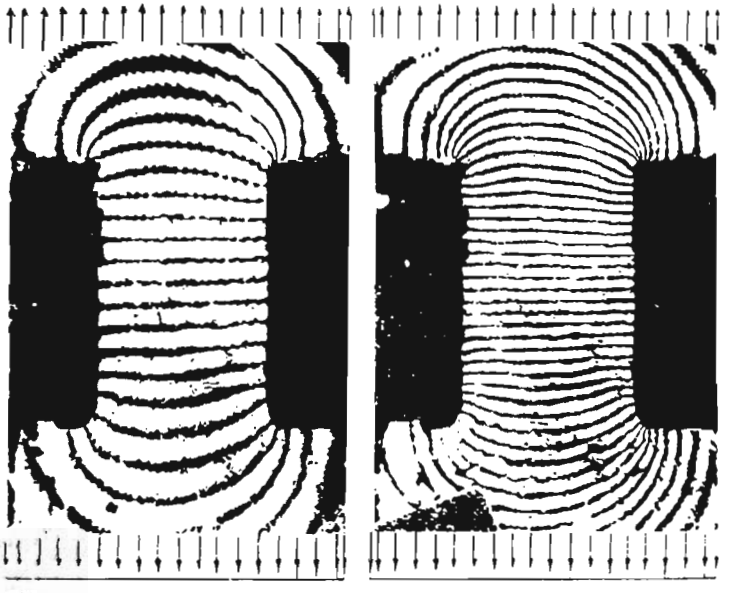

Fig. 12. Interference fringe patterns observed on transmission by reconstruction of the hologram, recorded at the surface of a metallized grating, having frequency 537 lines/mm at a stress value at the middle cross-section of the sample 44 and 88 MPa, respectively

To illustrate the above statement Fig.12 shows the interference fringe patterns corresponding to the lines of the level of the function $V+W(1-\cos\gamma)$. Interference patterns were photographed at $\gamma = 33^o$. The dimensions of the sample are given in Fig.13. The diagrams of the relative displacements at sample cross-section 1 are also shown here and they are designed on the basis of three experiments: the points, designated by circles and crosses are obtained after analysis of interference patterns as seen at the transmission at two strain levels at the middle cross-section

of the sample: 44 and 88 MPa respectively; the points designated by a triangle are obtained after analysing an interference pattern reconstructed from a hologram, recorded on the same surface of a sample, but before grating was applied, while the stresses at middle cross-section "0" was 44 MPa.

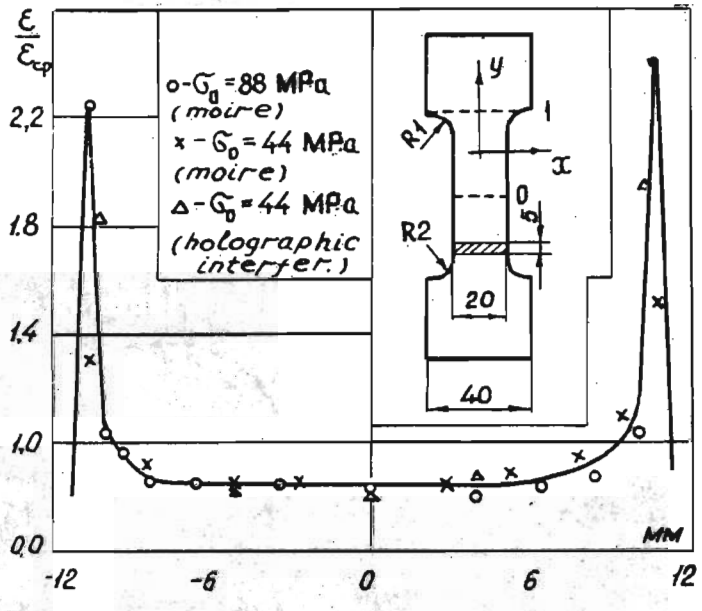

Fig. 13. Diagram of the strains ε_y at the cross-section 1 of the sample

Since the grating having frequency of 537 lines per mm was placed on the sample surface, then for interference patterns observed at the transmission by stresses 44 MPa ($\varepsilon = 6.5 \cdot 10^{-4}$, $\psi < [\psi] = 1230$ lines/mm), the error in determining strains exceeds 5% by far. This error diminishes when the load is doubled, in this case $[\psi] = 615$ lines/mm.

For the method of holographic interferometry (optical patterns are observed on reflection) the most advantageous angles of observation should not exceed 50°. However, we failed to fulfil this task due to a sharp decrease in light intensity on the reconstructed pattern.

For defining the fractional order of fringes while observing interference patterns in "real time" we could recommend a method of varying the conditions of sample illumination. For instance, a hologram of a non-strained sample is recorded under illumination by collimated beam of light while interference patterns are observed either in a converging or diverging spherical wave. Some typical interference patterns obtained under similar conditions of the observation and loading of a sample but using different wave fronts illuminating a strained surface are given in Fig.14.

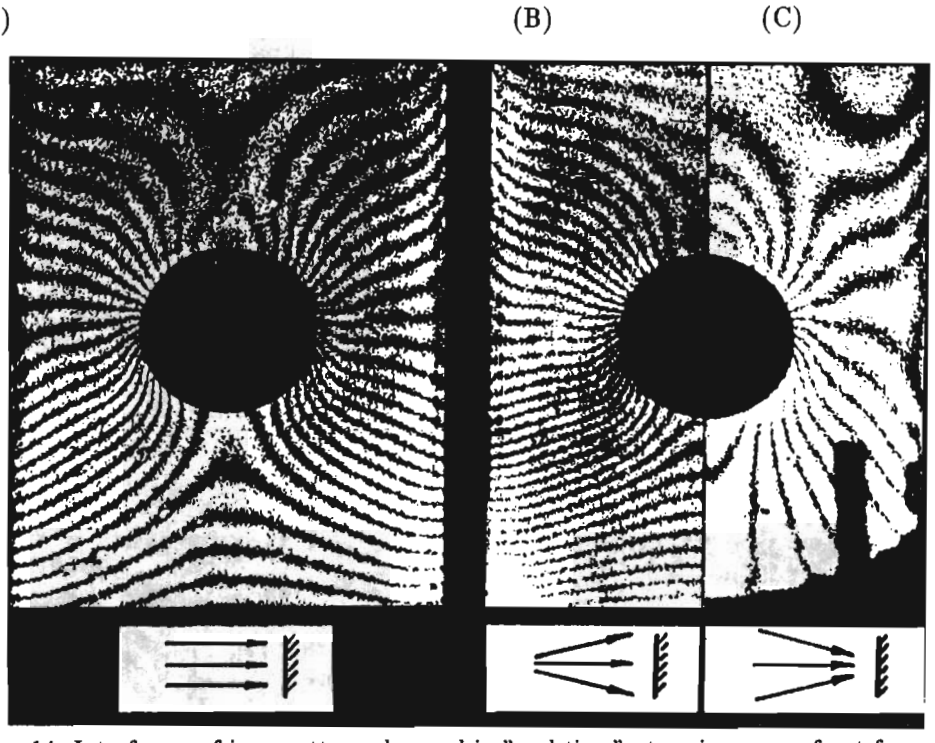

Fig. 14. Interference fringe pattern observed in "real time" at various wave front forms (the hologram of the non–strained sample is recorded under illumination by collimated beam of light

Fig.14A corresponds to collimated illumination beam, Fig.14B – to a converging wave and Fig.14C – to a diverging wave.

In the second case pseudo and real displacements agree in their sign, which leads to an increase of the spatial frequency of interference fringes, in the third example both pseudo and real displacements have different signs.

5.2. Analysis of the strain of a plate made of D16T aluminium alloy with a central round hole under axial load

5.2.1. Recording of double–exposure hologram on the sample surface without using any special reflecting coatings [17]. Dimensions of the sample under study and a diagram of strain are given in Fig.15. The load is acting along the y axis. Prior to the tests the surface of the sample was treated by fine abrasive paper in order to obtain the form of the diffusion indicatrice approximately to spherical.

The holograms were recorded on photoplates LOI–2 fixed on the sample sur-

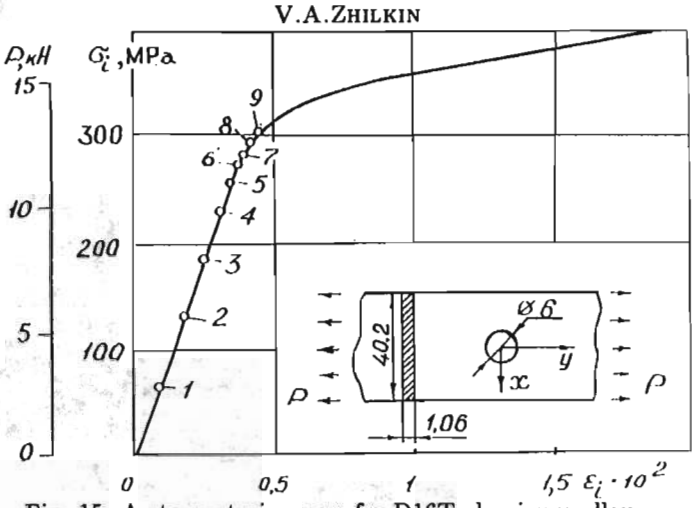

Fig. 15. A stress-strain curve for D16T aluminum alloy

(A)

(B)

(C)

Fig. 16. Photographs of the interference fringe patterns from the three loading stages as shown in the Fig.15: A – for the first, B – for the fifth, C – for the eighth step

face with the help of synthetic rubber SKTN–A. As a light source a HE–NE laser ($\lambda = 0.6328$ μm) 60 mW was employed. The check–up of the loading process was done according to readings of strain gages glued at two points: at some distance from the notch and in the vicinity of two critical points. The dots on the strain diagram correspond to the loading stages and to the registration of the double–exposure holograms. Fig.16 (A,B,C) shows photographs of fringe patterns observed on reflection corresponding to the first ($P = 2.8$ kN, $\Delta P = 2.8$ kN), fifth ($P = 10.9$ kN, $\Delta P = 1.2$ kN) and eighth ($P = 12.4$ kN, $\Delta P = 0.5$ kN) loading stages (P – full loading, ΔP – increment of load at one stage).

The quantitative analysis of the holographic interferograms was done for the first five loading stages and strain fields ε_x, ε_y, γ_{xy} were determined. Assuming $\mu = 0.5$ the intensity of strains ε_i was determined and then according to the general strain–stress curve the intensity of stresses σ_i was found.

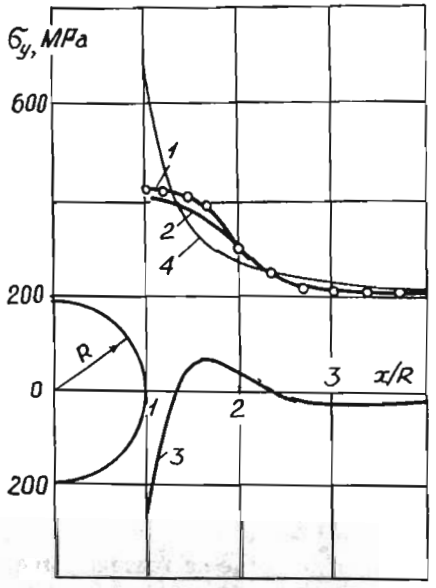

Fig. 17. Diagrams of stress σ_y in the critical cross–section of a sample for the fifth stage of its loading

The beginning of the plastic strain of the material was determined on the basis of Mises theory $\sigma_i = \sigma_T$. For the given example $\sigma_T = 333$ MPa, $\varepsilon_i = 6.67 \cdot 10^{-3}$. Fig.17 shows diagrams σ_y for a degree of plastic strain $\psi = 0.687$ obtained on the basis of the minor elastic–plastic strains and the flow theory by Saint Venan and Levy Mises (the coincidence of the diagrams was satisfactory, as it should be during a simple loading). The diagram of remaining stresses (3) at the critical cross–section of which was determined experimentally, while the other obtained according to formulae of the theory of elasticity (4) assuming an ideal elasticity of

the material of the object.

5.2.2. The recording of the double–exposure holograms at the surface coated by a metallized grating [12]. The dimensions of the sample and the net area containing 483 nodal points, along the lines of which we determined the strains ε_x, ε_y, γ_{xy}, and the strains ε_i, are given in Fig.18.

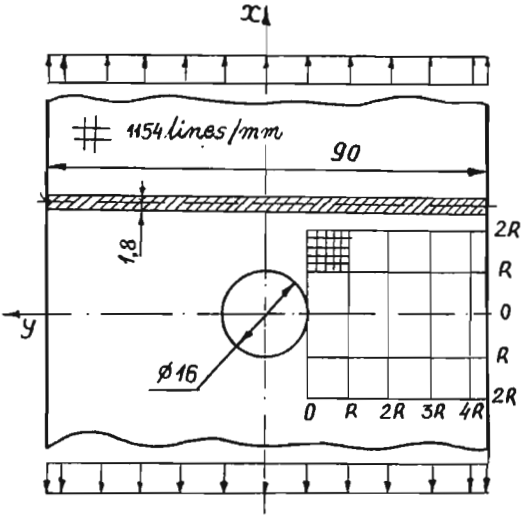

Fig. 18. The dimensions of the sample and the area of a grating

We have placed an orthogonal grating with frequencies $\psi_x = \psi_y = 1154$ lines/mm. The lines of the grating were oriented along the symmetry axes of the sample. The holograms were registered on photoplates PE–2. The sample was loaded in a standard testing machine UME–10TM. We have done 42 stages of loading. At the plastic stage of loading the second exposure of holographic plate was carried out only when the rate of the decrease of force could not influence the quality of interference patterns substantially.

Fig.21 shows the fragments of the interference patterns registered in plane yz. It illustrates the difference of the patterns observed on transmission (1) and on reflection (2). In these examples we can easily see that strains of type W influence the interference pattern type greatly, especially those observed on reflection.

5.3. Stress–strain curves under low cycle loading

There are two possible experimental ways to solve the problem. The first and the most general is to measure the strains on the plane of an object (U or V), and

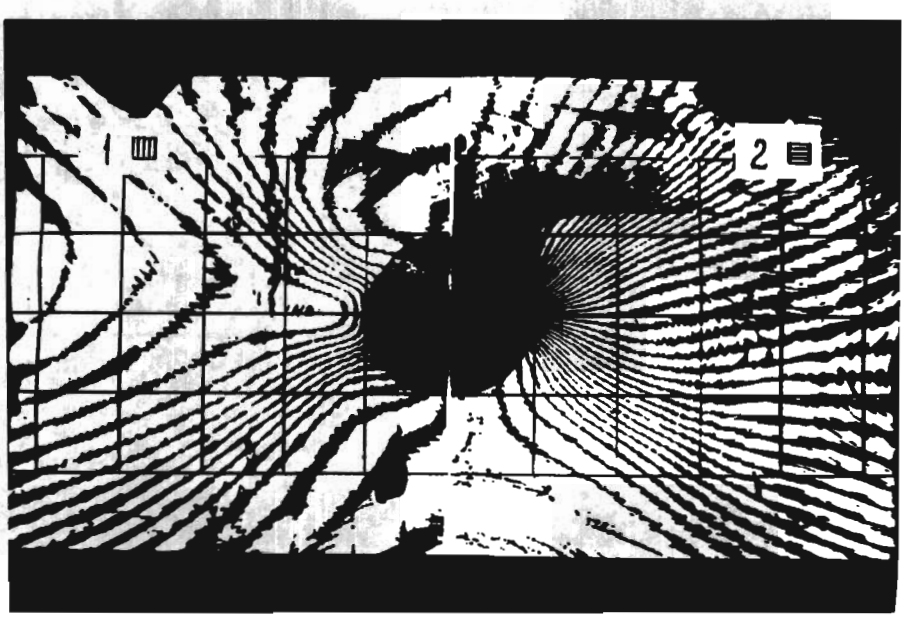

Fig. 19. Interference fringe patterns as seen on transmission in planes yz for the left and xz for the right part of the photograph

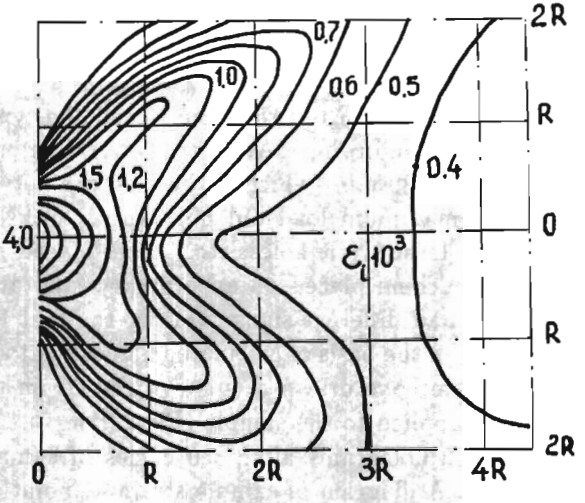

Fig. 20. Trajectory of the constant strain ε drawn according to the results of processing of interferograms (shown in Fig.19) $\mu = 0.5$

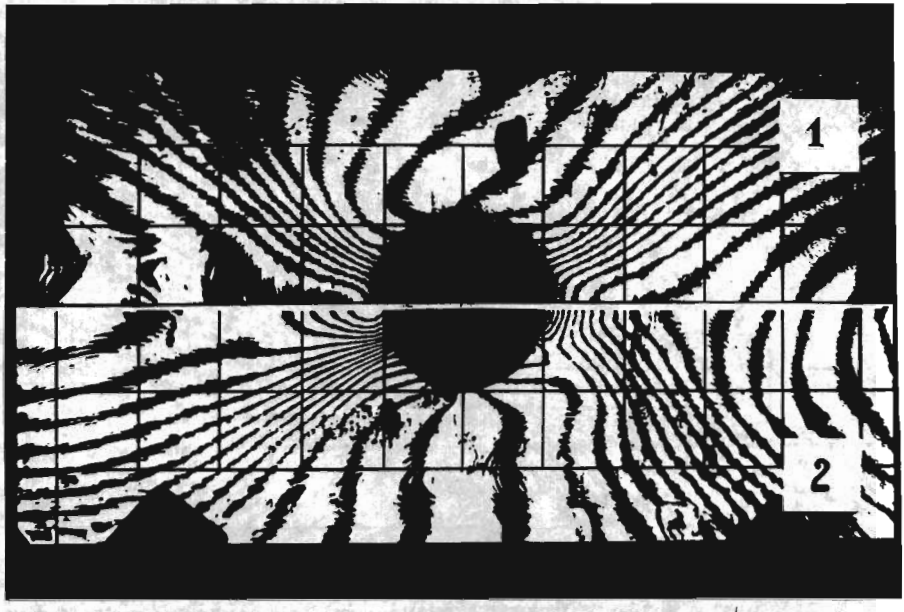

Fig. 21. Interference fringe patterns as seen in planes yz on transmission – 1, and on reflection – 2

the second one is based on measurements of the changes in the thickness of the sample in a zone of strain concentration, and assumption that the conditions of plane stress state is fulfilled.

5.3.1. Registering of displacements V (or U). The samples were made of sheet aluminum alloy D16T. The dimensions of the sample and the type of coordinate net placed on its surface are given in Fig.22A. To avoid buckling of the sample the length of the sample was $70 \div 80$ mm (which is the distance between the clamps of a loading device). The maximum load did not exceed 80 kN. The elements of the optical device (laser, lenses, pin–holes, etc.) were placed near a standard electromechanical testing machine placed on an ordinary laboratory table. The load applied to the sample had different signs. During the first loading cycle 23 holograms were registered. On the basis of calculated values ϵ_y at a point A having coordinates $x = R$, $y = 0$ we have drawn a curve of the strain as a function of sign–alternating loading P applied to the sample (Fig.22B).

Similarly we have got 22 holograms after 350 cycles of symmetrical loading with a peak value of 80 kN. A diagram of sample strain at point A at the 351–st cycle is given in Fig.22C. A comparison of the curves in Fig.22B and C shows an effect of hardening of D16T alloy.

5.3.2. Registering of displacements W [34]. Since a photoplate placed on the surface of a sample similar to the one described in section 5.3.1., with a round

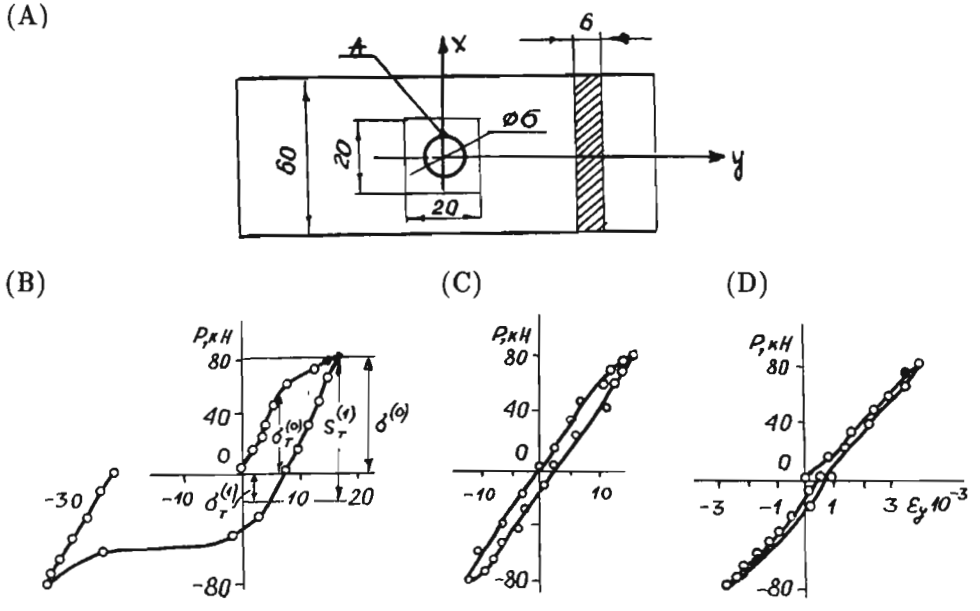

Fig. 22. The dimensions of the sample made of aluminum alloy D16T (A), diagrams of the strains of the three points of the sample (B,C,D)

notch, registers only local displacements $W_l = N\lambda/(2n)$, then the full displacements W can be determined by the formula

$$W = W_o + W_l = \frac{\mu h P}{2EF} + \frac{N\lambda}{2n}$$

where W_o represents displacements at a distance from the notch, μ – Poisson ratio for the material of a sample when it is loaded within the plastic limits, P – loading force, h – the thickness of a plate.

By a plane stress state

$$\varepsilon_y = -\frac{\varepsilon_z}{\mu^*} = -\frac{2W}{h\mu^*} \tag{5.5}$$

where μ^* is the transverse strain ratio beyond the plastic limit determined by approximate methods [35]. Using a stress–strain curve one draws a scheme of the dependency $\mu^* = f(\varepsilon_y)$, and then, assuming a random value of $\mu^* = \mu^{(1)}$, from the expression (5.5) the value of $\varepsilon_y^{(1)}$ is determined and according to the diagram $\mu^* = f(\varepsilon_y)$ values of $\mu^* = \mu^{(2)}$ found and so on. The process is repeated until the inequality

$$|\mu^{(n-1)} - \mu^{(n)}| < \Delta$$

is fulfilled, where Δ is an error in finding μ^* given by an experimenter.

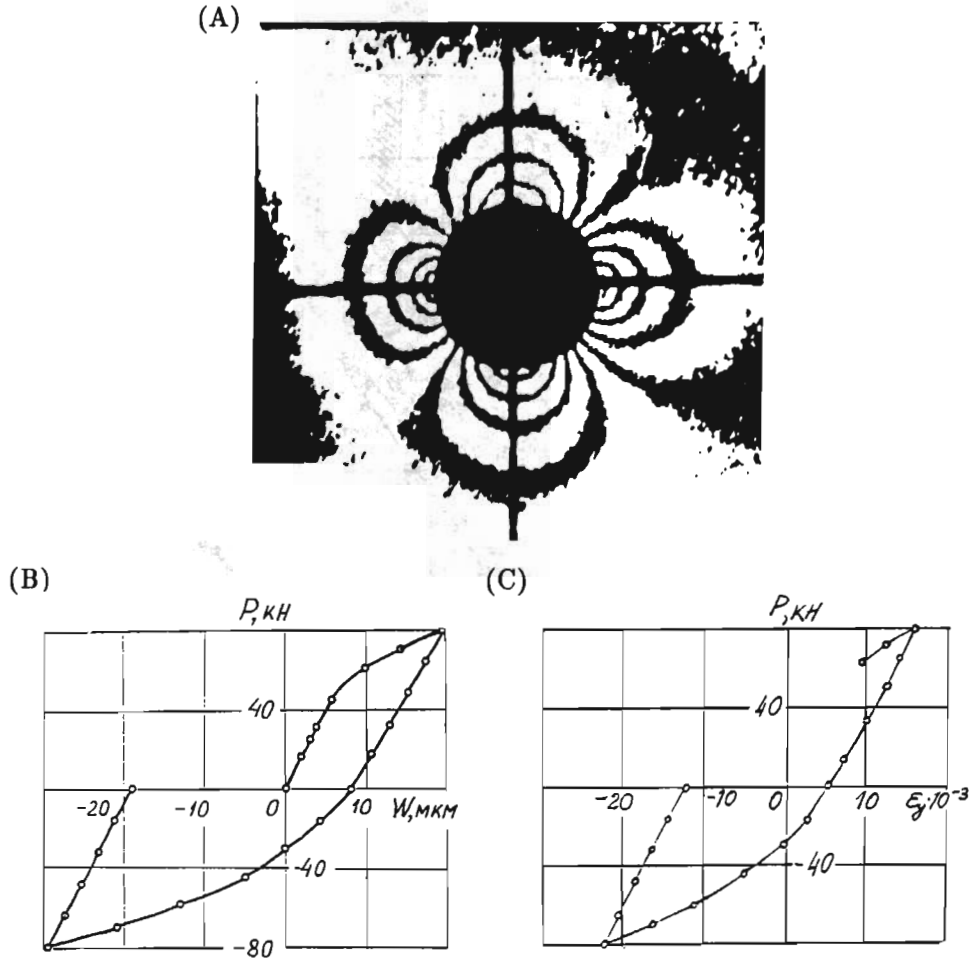

Fig. 23. Interference fringe pattern for the fourth stage of loading (A), diagram of W (B) and strain ε_y (C) for point A of the sample

Fig.23A shows the typical interference fringes for one of loading stages. Fig.23B shows displacement W as a function of load P, Fig.23C ε_y as a function of load plotted for point A of the sample described in the previous section.

The method of drawing of the diagrams of strain as a function of load for plane samples is contactless, it does not distort a field of plastic strain, and besides, is assures a considerable reduction of the time of processing interferograms as compared with the one described in section 5.3.1.

5.4. The study of strain of a pivot bearing in non–metallic structure (Fig.25) [11]

The upper and lower parts of a hinge are hollow, their walls are made of 15 mm thick plexi–glass AG–4C of types B and C. On the plane dimension are 75 × 220 mm. Stiffening ribs are placed between the longitudinal vertical walls of this structure, they strengthen zones of contact of the hinges with a cylindric pivot. The supporting hinge was loaded up to $P = 30$ kN and then a cross grating with a frequency of 912 lines/mm was placed on the surfaces, which consisted of 6 similar gratings 73 × 90 mm (on the upper edge of the hinge a linear grating was positioned). The orientation of the lines of the grating approximately corresponded to vertical and horizontal directions, gaps between the gratings not exceeding $1 \div 1.5$ mm.

Fig.24 shows interference fringes observed on transmission obtained by loading the hinge with a force $P = 20$ kN corresponding, at the first approximation, to the lines of the constant displacements V (Fig.24A) and to those of displacements U (Fig.24B). Strains ε_x and ε_y were determined at horizontal cross–sections of the hinges at a distance of 30 and 60 mm from the base (Fig.25A). Fig.25B shows diagrams of normal ε_n and tangential ε_θ strains along the surface of contact of the pivot and the hinges.

Parallel to the experimental studies the optimization of the dimensions of the supporting hinges on the basis of the numerical method was performed. Triangular elements were used, forming in space a surface coinciding with the middle surface of the hinge. For modelling a pivot the elements of higher rigidity were used, radially directed from the pivot axis. A mesh for the supporting hinge is shown in Fig.26.

A preliminary calculation, when a vertical load of 20 kN acted upon the hinge in absence of friction forces over the contact area, showed that results do not correspond with experimental ones. The lines of the constant displacements U (Fig.27A) and the fringe pattern given in Fig.24B do not correspond to each other quantitatively. Besides, the calculated vertical displacements were 40% greater than that obtained experimentally. In order to account the friction forces between the hinges and the base additional hinges were introduced, connecting the nodal points with the support and modelling the friction forces. Fig.27B shows isolines of horizontal displacements obtained with the view of the friction forces over the contact area of the hinge and the base. The isolines of the displacements in this case correspond perfectly to isolines of interference patterns. A divergence of the calculated vertical displacements and the experimental ones was reduced up to 15%. A corrected model of calculation was used for the optimization of the form of the pivot bearing.

(A)

(B)

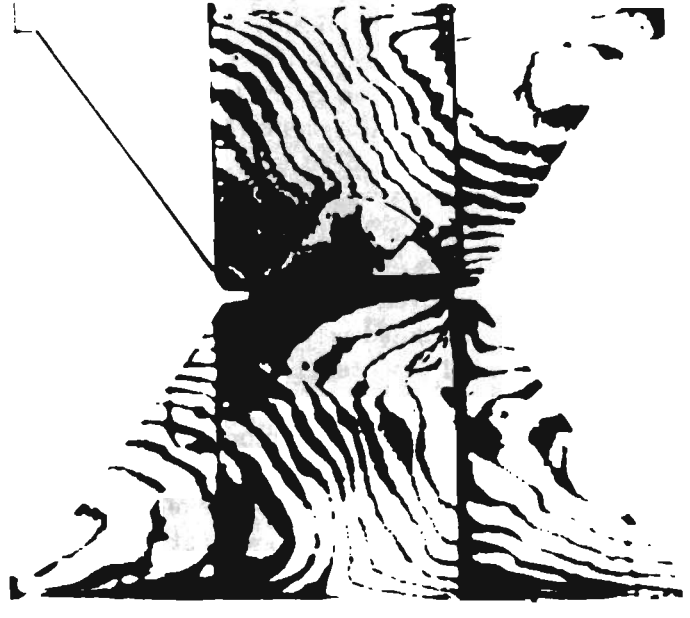

Fig. 24. Interference fringe patterns for the hinge, observation in the plane yz (A), and in the plane xz (B)

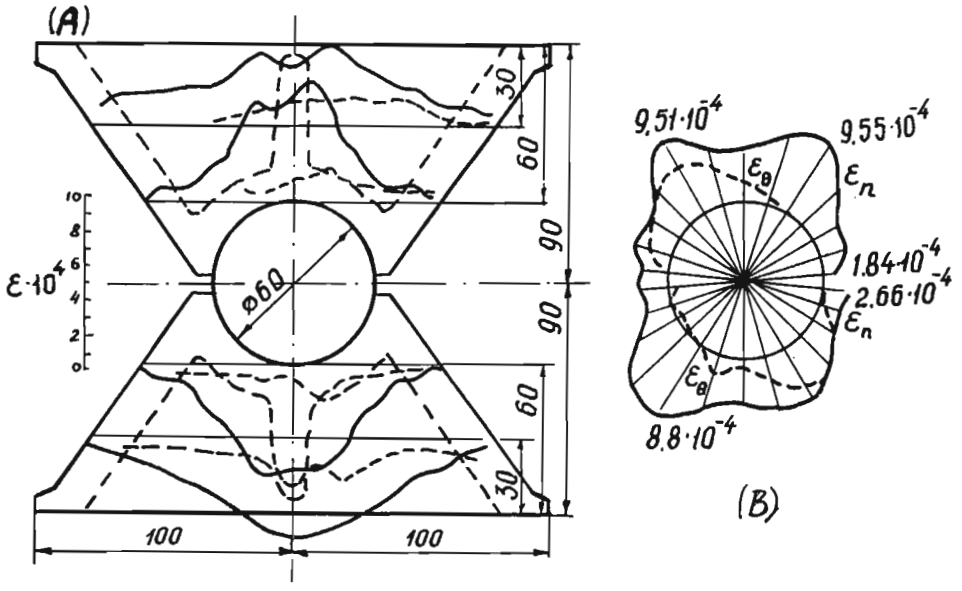

Fig. 25. Diagrams of the strain ε_x and ε_y in the cross-sections 1,2,3,4, (A), diagrams of the strain ε_n and ε_θ along the contact surface

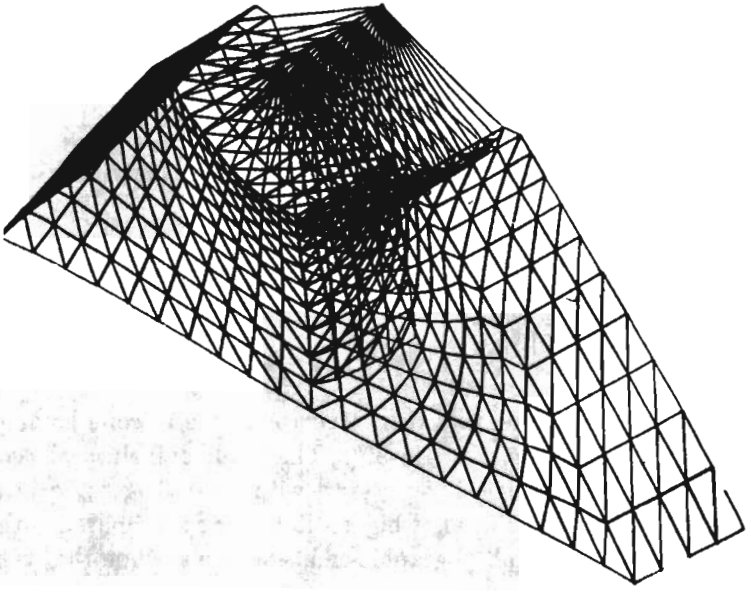

Fig. 26. Discretization of the hinge for FEM calculation

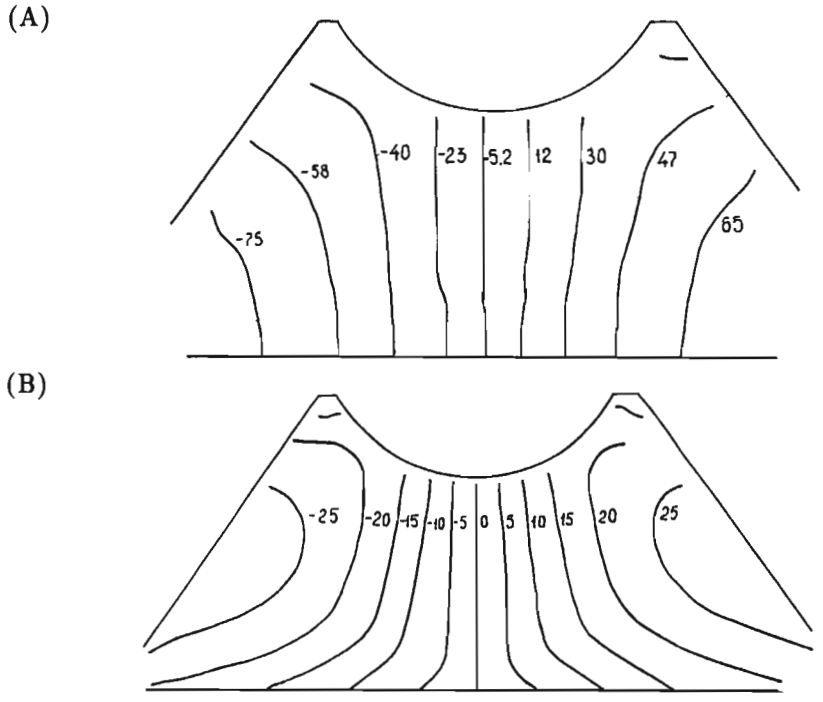

Fig. 27. Trajectory of the constant displacement u obtained from calculation for the case without friction on the contact between the hinge and support (A), and the same when friction was included (B)

Hence, the optical method can be successfully used for correcting the model of calculation.

5.5. The use of the panoramic interferometer for studying strain of round cylindrical shells [15]

A panoramic interferometer is a truncated round metal cone having an inner mirror–like surface and a vertex angle 90°. The studied shell is placed into the cone and the same can be done, if necessary, with an orthogonal grating placed on a glass cylinder having a somewhat bigger diameter as compared with the shell diameter (in the latter case a photographic emulsion is placed on the surface of the shell, what allows for recording the displacements U and V). To the wide base of the cone a photoplate PE–2 is fixed which registers, mainly, normal displacements W of the upper cover of the shell and its lateral surface.

A maximum size of the studied shell is defined by the dimensions of the cone

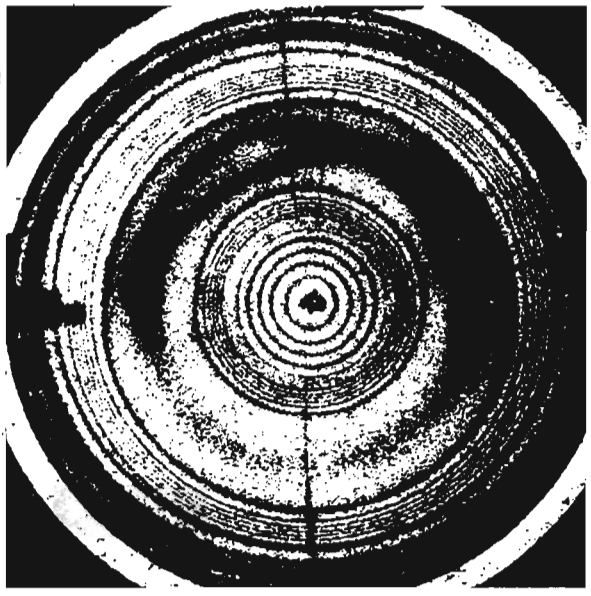

Fig. 28. Interference fringe pattern obtained by the use of pano ramic interferometer. for the deformation of the cy lindrical container

and by the level of its vibrations. When recording the displacements W vibrations of a photoplate are the most influential. In our experiments cones with maximum diameter 80 and 150 mm were used. Fig.28 shows a pattern of interference fringes obtained while loading a closed cylindrical shell under inner pressure.

The shell was made of plexi–glass. The bottom and the wall were machined on a lathe separately, then they were glued together.

Fig.29A shows diagrams of displacements W for the upper cover and Fig.29B for the lateral wall of the shell. A certain difference between the theoretical and the experimental results for the lateral wall of the shell was recognized as the influence of the yielding of a glued connection between the bottom and shell.

Fig.30 shows a moire pattern of fringes obtained under an axial compression of the shell made of plexi–glass (length – 37 mm, wall thickness – 1.0 mm, radius of the middle surface – 13.0 mm) with two round holes (radius 3.0 mm) and a force of 150 kN. The frequency of the used grating was 585 lines/mm. A pattern of moire fringes does not differ much from similar patterns obtained for plane wide sample, that is, the strain of the middle surface of a shell and a bar are similar. A maximum value of the concentration of membrane stresses determined by experiment was 3.4, while the theoretical value of the ratio is 3.44 [36].

(A)

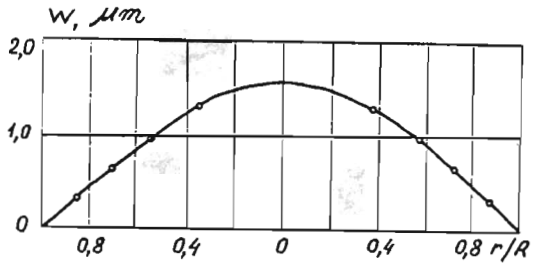

(B)

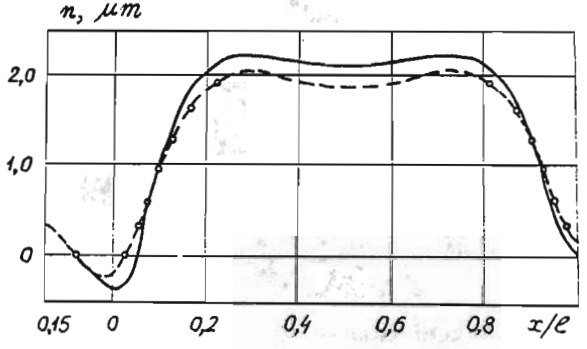

Fig. 29. Diagram of deformation w for the head of the container (A), radial displacement n for points along generator, solid line according theoretical calculations, dash line according experiments

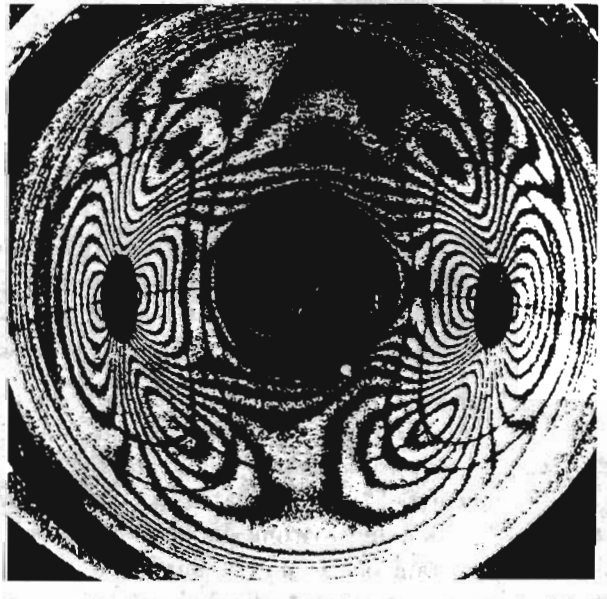

Fig. 30. Interference fringe pattern obtained by use panoramic interferometer for the cylinder with notches

References

1. DENISYUK YU.N., *Ob otobrazhenii fizicheskikh svoĭstv ob'ekta v volnovom pole rasseyannogo im izlucheniya,* Dokl.AN SSSR, **144**, No.6, 1962, 1275-1278

2. ZHILKIN V.A., POPOV A.M., *Issledovanie deformirovannogo sostoyaniya ploskikh obrazcov metodom golograficheskogo muara,* Izv.Vuzov, Str-vo i Arkhitektura, No.9, 1979, 50-53

3. NEUMAN D.B., PENN R.C., *Object motion compensation using reflection holografy,* J.Opt.Soc.Amer., **62**, No.12, 1972

4. BOONE P.M., *Use of reflection kholograms in kholografic interferometry and speckle correlation for measurement of surface displacement,* Optica Acta, **22**, No.5, 1975, 579-589

5. ZHILKIN V.A., GERASIMOV S.I., *Study of deformed samples using and interferometer attached to the sample,* Sov.J.Tech.Phys., **27**, No.10, 1982, 1270-1279

6. ZHILKIN V.A., BONDARENKO A.N., *Issledovanie smyatiya drevesiny v otverstii metodom spekl-interferometrii,* Izv.Vuzov, Str-vo i Arkhitektura, No.10, 1979, 44-47

7. ZHILKIN V.A., ZINOV'EV V.B., *Vozmozhnye metody rasshifrovki golograficheskikh ob'emnykh interferogramm, zapisannykh u poverkhnosti metallizirovannykh rastrov,* Mekh.Deformiruemogo Tela i Raschet Transp. Sooruzheniĭ, Novosibirsk, 1980, 113-120

8. ZHILKIN V.A., *Interference optical method of eshamining the deformed state,* Int. Lab., 47 (10), 1981, 1059-1067

9. ZHILKIN V.A., ZINOV'EV V.B., ADYLOV A.K., *Metodika issledovaniya deformirovannogo sostoyaniya sterzhnevykh kleevykh soedineniĭ metodom golograficheskogo muara,* Izv.Vuzov, Str-vo i Arkhitektura, No.7, 1982, 133-137

10. ZHILKIN V.A., BORYNYAK L.A., *Issledovanie deformirovannogo sostoyaniya zamknutoĭ krugovoĭ cilindricheskoĭ obolochki metodom golograficheskoĭ interferometrii,* Mekh.Deformiruemogo Tela i Raschet Transp.Sooruzheniĭ, Novosibirsk, 1982, 85-89

11. ZHILKIN V.A., ZINOV'EV V.B., GORBUNOVA T.V., *Issledovanie anizotropnykh zadach mekhaniki deformiruemykh tel metodom golograficheskogo muara,* Mekh. Kompoz.Materialov, No.2, 1983, 341-347

12. ZHILKIN V.A., *Investigation of elastoplastic problems by the method of holographic moire,* Probl.Prochn., No.12 (186), 1984, 69-76

13. ZHILKIN V.A., GERASIMOV S.I., *Primenenie nakladnogo golograficheskogo interferometra dlya opredeleniya uprugoplasticheskikh i ostatochnykh deformaciĭ,* Ostat. Tekhnol.Napryazh., Tr. 2 Vses.Simpoziuma M., 1985, 136-141

14. ZHILKIN V.A., ZINOV'EV V.B., *Opredelenie zony kraevogo éffekta s pomoshch'yu metoda golograficheskogo muara,* Zh.Prikl.Mekh.i Tekhn.Fiz., No.5, 1986, 132-135

15. ZHILKIN V.A., USTIMENKO A.P., BORYNYAK L.A., *Study of the strain state of thinwalled circular cylindrucal-shell using a panoramic interferometer,* Sov. Ap.Mech., **22**, No.12, 1986, 1177-1181

16. ZHILKIN V.A., SHEVTSOV R.G., KOSENYUK V.K., RAKIN A.S., *Issledovanie napryazheniya v shiftovykh soedineniyakh golograficheskim muarovym metodom,* Probl.Prochn., No.12, 1987, 74-77

17. GERASIMOV S.I., ZHILKIN V.A., *Issledovanie ploskikh uprugoplasticheskikh zadach metodom golograficheskoĭ interferometrii*, Zh.Prikl.Mekh.i Tekhn.Fiz., No.2, 1988, 107-116

18. ZHILKIN V.A., *An elastoplastic problems investigation with the help of help of methods based on holographic recording of information*, Int.Conf.Measurement of Static and Dynamic Parameters of Structures and Materials, Plzen, 1987, **2**, 627-632

19. HOWLAND R.C.J., *On the stresses in the neighborhood of a circular hole in a strip under tension*, Phil.Trans.Roy.Soc., **229** (Ser.A), 1929, 49-86

20. ZHILKIN V.A., GERASIMOV S.I., SARNADSKIĬ V.N., *Otsenka Tochnosti opredeleniya peremeshcheniĭ s pomoshch'yu nakladnogo golograficheskogo interferometra*, Optika i Spektroskopiya, **62**, No.6, 1987, 1385-1389

21. ZHILKIN V.A., ZINOV'EV V.B., *Decoding of interference pictures in the holographic -moire technique*, Zh.Tehn.Fiz., **56**, No.1, 1986, 113-118

22. ZHILKIN V.A., ZINOV'EV V.B., *Issledovanie poleĭ peremeshcheniĭ v élementakh transportnykh soopuzheniĭ metodom spekl-fotografii*, Napryazheniya i deformacii v zh.-d. konstrukciyakh, Novosibirsk, 1988, 49-53

23. KLIMENKO I.S., KRIVKO T.V., MALOV A.H., RYABUKHO V.P., *Spekl-interferometriya prodol'nogo smeshcheniya s ob'emnoĭ registracieĭ spekl-struktur*, Zh. Tekhn. Fiz., **58**, No.1, 1988, 182-186

24. ZHILKIN V.A., BONDARENKO A.N., *Opredelenie peremeshcheniĭ nedeformiruemykh zhestkikh tel metodom spekl-interferometrii*, Izv.Vuzov, Str-vo i Arkhitektura, No.6, 1977, 143-148

25. CHIANG F.P., ASUNDI A., *Perspective effect in the white light speckle method*, Appl. Opt., **21**, No.10, 1982, 1708-1710

26. TIMOSHENKO S.P., GUD'ER DZH., *Teoriya uprugosti. M.*, Nauka, Moskva 1979

27. GERASIMOV S.I., GUZHOV V.I., ZHILKIN V.A., KOSACHOK A.G., *Automated processing of interference patterns in investigations of strain fields*, Int.Lab., **51**, No.4, 1985, 389-392

28. ZHILKIN V.A., KOSENYUK V.K., ZINOV'EV V.B., *Use of boundary integral equations in decphering interference patterns*, Mechanics of Composite Materials, **24**, No.1, 1988, 136-141

29. TIMOSHENKO S.P., *Prochnost' i kolebaniya élementov konstrukciĭ. M.*, Nauka, Moskva 1975

30. ZHILKIN V.A., *Method of approximating order functions of interference-fringes in optical method*, Industrial Laboratory, **48**, No.10, 1982, 1012-1016

31. ZHILKIN V.A., *Ocenka chuvstvitel'nosti rastrovykh i interferencionnykh preobrazovateleĭ pri issledovanii lokal'no deformirovannykh zon*, Zavodskaya Laboratoriya, **46**, No.6, 1980, 548-551

32. SIRATORI M., MIESI T., MACUSIMA H., *Vychislitel'naya mekhanika razrusheniya. M.*, Mir, 1986

33. BIRGER I.A., *Ostatochnye napryazheniya. M.*, Mashgiz, 1963

34. ZHILKIN V.A., GERASIMOV S.I., *Postroenie diagrammy ciklicheskogo deformirovaniya ploskikh obrazcov po dannym metoda golograficheskoĭ interferometrii*, Zavodskaya Laboratoriya, **55**, No.5, 1989, 57-62

35. MALININ N.N., *Prikladnaya teoriya plastichnosti. M.*, Mashinostroenie, 1968

36. LUR'E A.I., *Statika tonkostennykh uprugikh obolochek. M.; L.*, OGIZ, GITTL, 1947

Zastosowanie nakładanych interferometrów holograficznych w mechanice eksperymentalnej

Streszczenie

Autor przedstawia w pracy przegląd metod różnych problemów mechaniki przy pomocy nakładanych interferometrów holograficznych. Badania przeprowadzane były w Instytucie Transportu Kolejowego w Nowosybirsku oraz w Instytucie Modernizacji i Elektryfikacji Rolnictwa w Czelabińsku. W pracy omówiono zarówno tradycyjne, jak i nowe metody analizy obrazów interferometrycznych otrzymanych z hologramu utrwalonego w odległości kilku centymetrów od powierzchni obiektu. Podano przykłady ilustrujące metody otrzymywania pól odkształceń zarówno elastycznych jak i plastycznych. Badano naprężenia osiowe w taśmach z koncentratorem obciążonych statycznie bądź cyklicznie małą liczbą cykli oraz struktury powłokowe obciążone osiowo bądź ciśnieniem wewnętrznym.

Praca wpłynęła do Redakcji dnia 10 października 1990 roku